A Microstrip Lowpass Filter With Wide Tuning Range and Sharp Roll-Off Response

Gholamhosein Moloudian, Siroos Bahrami, and Raheel M. Hashmi

***Abstract*—In this brief, a compact lowpass filter (LPF) with wide stopband, very sharp roll-off response and wide tuning range is presented for microwave diode detector applications. It employs two hexagonal-shaped resonators and multiple open-end stubs as suppression cells. The results of the proposed hexagonal-shaped resonator and LC circuits are in good agreement. The 3 dB cut-off frequency for the proposed LPF is 2.2 GHz and the roll-off-rate (ROR) parameter for the proposed LPF is very sharp and equal to 308.6 dB/GHz. Furthermore, insertion loss (IL) and return loss (RL) in the passband region are better than 0.3 dB and 18 dB, respectively. Moreover, the stopband is wide, ranging from 2.34 to 18 GHz, with a 22 dB rejection level. The tuning range of 3 dB cut-off frequency is also wide, equal 0.48 to 1.7 GHz (71%). As an application demonstrator, an envelope detector was designed and fabricated. The proposed detector (with LPF) highly suppresses any harmonics of the fundamental frequency. The proposed LPF and microwave detector is designed, simulated, fabricated and measured. The results of simulation and measurement are in good agreement.**

***Index Terms*—Diode detector circuit, feature selective validation, sharp response, tunable lowpass filter.**

I. Introduction

RF/MICROWAVE lowpass filters (LPFs) are used in most telecommunication systems for the suppression of harmonics and unwanted signals. LPF is usually essential in the diode-based microwave devices and circuits such as mixers, multipliers, and detectors. Emerging applications such as wireless communications continue to challenge filters with compact size, sharp roll-off rate (ROR), wide stopband, high suppression factor (SF), low insertion loss (IL), high relative stopband (RSB), and high figure-of-merit (FOM) [1]. In recent years, various resonators with different geometries and structures have been offered to design compact filters with good performance [2]–[13]. A compact filter with wide stopband and good performance is presented in [2]. Moreover, in [3], multi open stubs are used to provide LPF, but ROR is poor. To obtain expanded stopband defected ground structure (DGS) has been used to provide LPF [4]–[6]. Also, the compact LPF proposed in [7] used a T-shaped resonator and results show low IL in the passband and wide stopband.

All the filters reviewed in the articles above [2]–[7] are not tunable. With the development of the RF/Microwave telecommunication systems, the need for tunable filters has been increased. In general, a limited number of articles [8]–[12] has proposed tunable filters. Furthermore, in [9]–[11], a tunable LPF with a wide stopband is proposed. Furthermore, a varactor-tuned LPF with a large cutoff frequency tuning range and a sharp ROR response is presented in [12], but bandwidth stopband is low.

In this brief, an LPF using hexagonal shaped resonator with compact size, sharp ROR, wide stopband, high SF, and low IL is proposed. Furthermore, another tunable LPF with a wide tuning range for 3 dB cut-off frequency is integrated with the envelope detector structure. By changing the bias voltage, harmonics can be controlled for each carrier frequency separately. Its wide tuning range is a significant advantage over prior art as it provides control over the harmonics suppression level. To the best of the authors' knowledge, tunable LPF is considered for the first time as the harmonics controller in the envelope detector.

II. Design and Equivalent Circuit Modeling of the LPF and its Configuration

As a primary step, we start with designing a basic rectangular resonator based on the guidelines mentioned in [1] as illustrated in Fig. 1(a). The 3dB cut-off frequency is fixed to 2GHz. One of the important parameters of LPF is the rate of change from passband to stopband (ROR). To calculate the ROR parameter, the following equation is used [14].

$$\mathrm{ROR} = \frac{\alpha_{max} - \alpha_{min}}{f_s - f_c}\left(\frac{\mathrm{dB}}{\mathrm{GHz}}\right) \tag{1}$$

In this equation, α_{max} is usually -40 dB and α_{min} is -3 dB; f_s is the frequency of -40 dB point, and f_c is the cut-off frequency. The ROR parameter of the basic resonator is not satisfactory. Thus, to achieve sharper ROR, hexagonal-shaped resonators [5] in the single and double form shown in Fig. 1(a) are investigated. The equivalent circuit which is used in the analysis of the hexagonal resonator is also provided in Fig. 1(a). The transfer function for this equivalent circuit is as follows:

$$\frac{v_{out}}{v_{in}} = \frac{a_2 S^4 + a_1 S^2 + a_0}{b_5 S^5 + b_4 S^4 + b_3 S^3 + b_2 S^2 + b_1 S + b_0} \tag{2}$$

where S is the complex frequency and constants a_i, b_i are related to equivalent circuit parameters (3), as shown at the

Manuscript received March 9, 2020; accepted March 29, 2020. Date of publication April 2, 2020; date of current version November 24, 2020. This work was supported in part by the Australian Research Council. This brief was recommended by Associate Editor I. W. H. Ho. *(Corresponding author: Raheel M. Hashmi.)*

Gholamhosein Moloudian and Siroos Bahrami are with the Electrical Engineering Department, Salman Farsi University of Kazerun, Kazerun 12345678, Iran.

Raheel M. Hashmi is with the School of Engineering, Macquarie University, Sydney, NSW 2109, Australia (e-mail: raheel.hashmi@mq.edu.au).

Color versions of one or more of the figures in this article are available online at https://ieeexplore.ieee.org.

Digital Object Identifier 10.1109/TCSII.2020.2985206

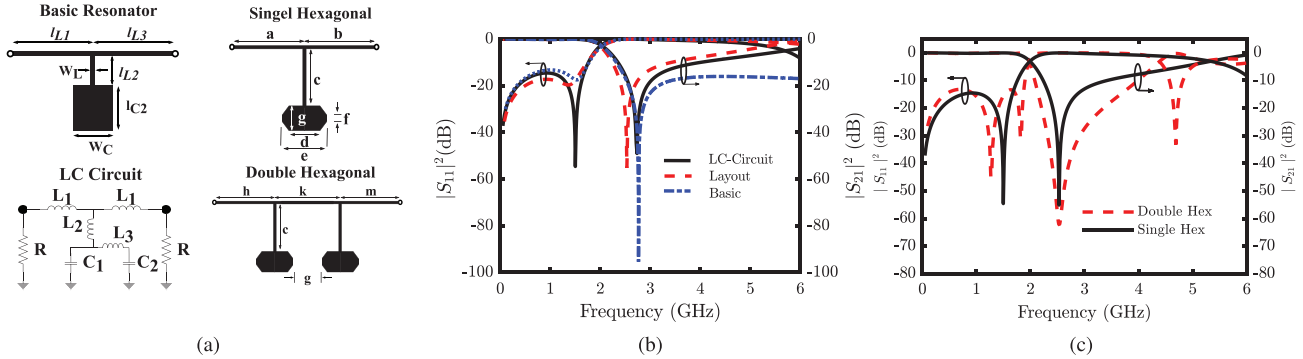

Fig. 1. (a) Basic resonator, single resonator, LC circuit of single resonator, and double hexagonal resonator design ($L_1 = 3.3$ nH, $L_2 = 3.4$ nH, $L_3 = 0.1$ nH, $C_1 = 0.3$ pF, and $C_2 = 1$ pF), and topology (Units: mm, $l_{L1} = 5.8$, $l_{L2} = 4.42$, $l_{l3} = 9.44$, $W_C = 4$, $W_L = 0.4$, $l_{C2} = 5.46$, a = b = 8, c = 7, d = 3.4, e = 6, f = 0.6, g = 3.2, h = m = 8, k = 12), (b) simulation results for different modeling of single hexagonal resonator, (c) single and double hexagonal resonators' simulation results.

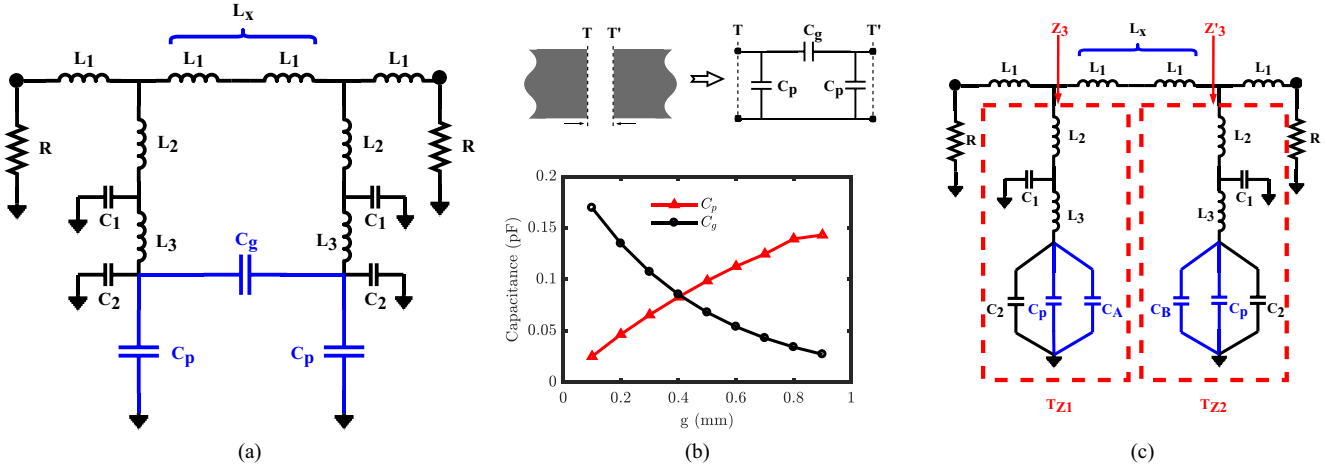

Fig. 2. (a) LC circuit for two series hexagonal shaped resonator, (b) variations of C_g and C_p with g, (c) Simplified equivalent LC circuit.

bottom of the page. The location of TZ can be obtained by finding zeros of (2).

$$f_z = \frac{1}{2\pi}\sqrt{\frac{\sqrt{a_1^2 - 4a_2} - a_1}{2a_2}} = 2.518\text{GHz} \tag{4}$$

Fig. 1(b) illustrates s-parameters of the rectangular and the single hexagonal resonators. There is a good agreement between the results of the hexagonal shaped resonator and LC circuit. According to this figure, the ROR parameter for the basic resonator and the hexagonal-shaped resonator are 56.5 and 77.4 dB/GHz, respectively. Therefore, the hexagonal resonator providers higher ROR in comparison to the rectangular resonator. To achieve the narrow transition band and even sharper ROR parameter, the double hexagonal resonators could be used. S-parameters of the single and double hexagonal resonators are compared in Fig. 1(c). Obviously, the ROR parameter of the double hexagonal resonator (88.73 dB/GHz) is better than that of the single hexagonal. Since the double hexagonal resonator provides better response the focus is now on the design procedure and analysis of this structure by providing its LC equivalent circuit as shown in Fig. 2(a). The microstrip gap (g) between two hexagonal resonators has a major effect on the transfer function. As shown in Fig. 2(b), the gap can be represented by a capacitive π-network. The shunt and series capacitances C_p and C_g may be determined based on the guideline given in [13], however the validity of those expressions is within $0.5 \leq W/h \leq 2.5$ and $2.5 \leq \varepsilon_r \leq 15$ [1]. Therefore, for the sake of accuracy, the shunt and series capacitances C_p and C_g may be determined based on the following equations [15]:

$$C_p = C_1\left(\frac{Q_2 + Q_3}{Q_2 + 1}\right) \times 10^{12}(pF) \tag{5}$$

$$C_g = 0.5hQ_1 exp(-1.86(\frac{g}{h}))v(pF) \tag{6}$$

where auxiliary quantities Q_i and v are defined in [15], g is the space between lines (gap) and W is the line width of two hexagonal resonators (W = 5.6 mm). Substitution of the substrate Rogers RO4003c parameters (h = 0.8128 mm, ε_r = 3.38, tanδ = 0.0022) results in $C_p = 0.13$ pF and $C_g = 0.034$ pF. The variations of C_g and C_p with respect to g are shown in Fig. 2(b). According to Fig. 2(b), one may conclude that by

$$a_0 = R,\quad a_1 = R(L_2C_1 + L_2C_2 + L_3C_2),\quad a_2 = RC_1C_2L_2L_3,\quad b_0 = R + 1$$
$$b_1 = 2L_1,\quad b_2 = a_1/R,\quad b_3 = (C_1 + C_2)L_1^2,\quad b_4 = a_2/R + RC_1C_2L_1L_3,\quad b_5 = C_1C_2L_1^2L_3 \tag{3}$$

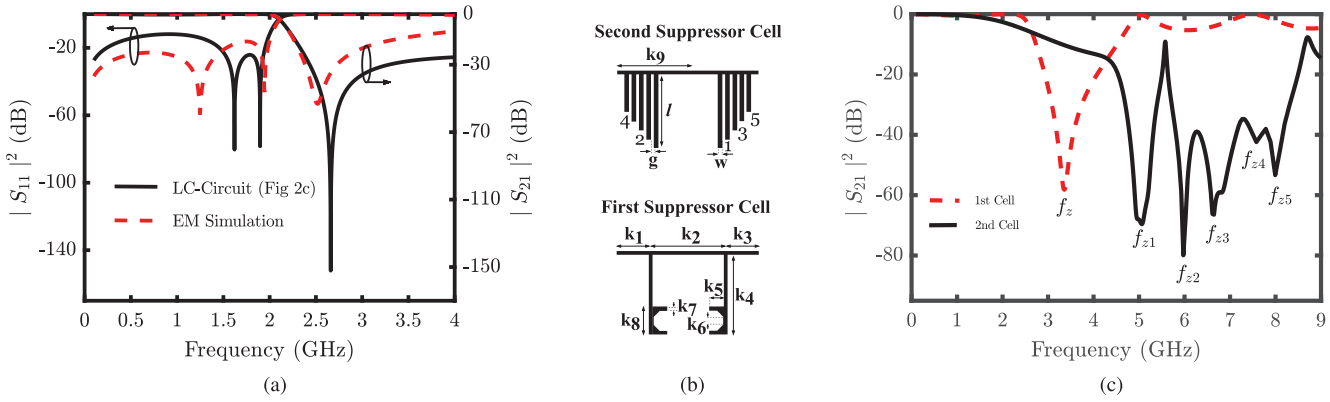

(a) (b) (c)

Fig. 3. (a) Simulation results of LC circuit and proposed resonator, (b) suppressor cells; first suppressor cell ($k_1 = 6$ mm, $k_2 = 13.4$ mm, $k_3 = 6$ mm, $k_4 = 11.5$ mm, $k_5 = 1.8$ mm, $k_6 = 1.8$ mm, $k_7 = 0.4$ mm, $k_8 = 4.4$ mm); second suppressor cell ($k_9 = 12.6$ mm, $l_1 = 10.2$ mm, $l_2 = 9$ mm, $l_3 = 7.8$ mm, $l_4 = 6.8$ mm, $l_5 = 5.8$ mm, w = 0.6 mm, and g = 0.4 mm), (c) Simulation results for suppressor cells.

adjusting line's spacing C_g and C_p capacitors could be controlled. A simplified version of the LC circuit as shown in Fig. 2(c) can be approximated by using the Miller effect.

$$L_x = 2L_1 \tag{7}$$

$$C_A = C_g(1 - \frac{V_B}{V_A}) \tag{8}$$

$$C_B = C_g(1 - \frac{V_A}{V_B}) \tag{9}$$

By extracting the transfer function in the simplified LC circuit, one can calculate C_A and C_B capacitors as well. The transfer function for the simplified LC circuit in Fig. 2(c) is obtained as follows:

$$\frac{v_{out}}{v_{in}} = \frac{1}{\zeta\xi + \zeta\frac{Z_T}{R} + \xi\frac{Z_T}{R} + \frac{Z_T}{Z_3}} \tag{10}$$

$$\zeta = 1 + \frac{j\omega L_1}{Z_3} \tag{11}$$

$$\xi = 1 + \frac{j\omega L_1}{\acute{Z}_3} \tag{12}$$

$$Z_3 = j\omega L_2 + (j\omega L_3 + \frac{1}{j\omega C_x}) \| \frac{1}{j\omega C_1} \tag{13}$$

$$\acute{Z}_3 = j\omega L_2 + (j\omega L_3 + \frac{1}{j\omega C_y}) \| \frac{1}{j\omega C_1} \tag{14}$$

$$Z_T = 2j\omega L_1 - \frac{\omega^2 L_1^2}{Z_3} \tag{15}$$

$$\acute{Z}_T = 2j\omega L_1 - \frac{\omega^2 L_1^2}{\acute{Z}_3} \tag{16}$$

where $C_x = C_2 + C_p + C_A$ and $C_y = C_2 + C_p + C_B$. Extracting TZ of the transfer function (10) gives

$$f_z = \frac{1}{2\pi}\sqrt{\frac{L_3C_x - L_2(C_1 + C_2) \pm \sqrt{k}}{2L_2C_1L_3C_x}} \tag{17}$$

where,

$$k = 2C_xL_2(C_1(L_3 + L_2) - C_xL_3) + L_2^2(C_1^2 + C_2^2) + L_3^2C_x^2 \tag{18}$$

Based on these equations, the location of TZ can be controlled by C_2, L_3, C_A, C_B, C_p and L_2. However, a more straightforward approach to determine the TZs is to find the roots of $\Im m\{Z_3\}$ or $\Im m\{Z_3'\}$. Thus, neglecting C_1 results in:

$$f_{z1} = \frac{1}{2\pi\sqrt{(L_2 + L_3)C_x}} \tag{19}$$

$$f_{z2} = \frac{1}{2\pi\sqrt{(L_2 + L_3)C_y}} \tag{20}$$

TABLE I
COMPARISON BETWEEN CALCULATED AND SIMULATED RESULTS FOR TRANSMISSION ZERO (*TZ*)

TZ	EM Simulation	Equations 19 and 20	LC-Circuit
	2.51 GHz	2.7 GHz	2.64 GHz

The values of the LC circuit for the proposed resonator are $L_1 = 3.1$ nH, $L_2 = 3.0$ nH, $L_3 = 0.25$ nH, $C_1 = 0.1$ pF, $C_p = 0.13$ pF, $C_g = 0.036$ pF, and $C_2 = 0.85$ pF. The calculated and simulated results for C_g are 0.034 pF and 0.036pF, respectively. There is a minor difference in results (0.002 pF) and agreement between the calculated and simulated results is acceptable. The comparison between the simulation results of the LC circuit (in Fig. 2(c)) and the EM simulation of the double hexagonal resonator are illustrated in Fig. 3(a). According to Fig. 3(a), the double hexagonal resonator has a TZ at 2.51 GHz (with −59.2 dB) and the LC equivalent circuit has TZ at 2.64 GHz (with −155.16 dB). Hence, there is a good agreement between the simulation results of the proposed resonator and the equivalent LC circuit. The calculated and simulated results for TZ of the proposed resonator are compared in Table I.

III. IMPROVING STOP-BAND AND DESIGN OF SUPPRESSOR CELLS

To achieve wide stopband, a series of suppressor cells as in Fig. 3(b) were added to the proposed resonator. The first suppressor cell is composed of two inverted-F shape resonators with transfer zero f_z. The second suppressor cell is composed of five stubs with different lengths and distinct TZs (f_{zi}). The simulation results of the first and second suppressor cells are shown in Fig .3(c) where the corresponding f_{zi} are also depicted. The simulation and measurement results of the proposed LPF are illustrated in Fig. 4. The 3 dB cut-off

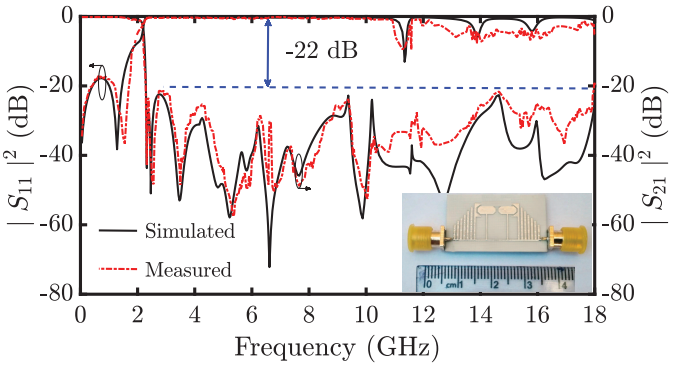

Fig. 4. Proposed LPF; simulated and measured results; fabricated sample.

TABLE II
COMPARISON OF THE PROPOSED LPF WITH PREVIOUS WORKS

Refs	f_c (GHz)	ROR (dB/GHz)	RSB	SF	NCS (λ_g^2)	IL (dB)	FOM
This work	2.24	308.3	1.54	2.2	0.36×0.16	0.3	18134
[3]	1.9	37	1.45	1.8	0.4×0.23	0.3	1050
[4]	1.9	85	1.43	2.5	0.13×0.23	0.5	10163
[5]	2.45	100	1.54	2	0.31×0.16	0.85	6210
[6]	1	78	—	2	0.16×0.1	0.3	—
[7]	2.68	42.5	1.51	2	0.16×0.15	0.12	5348

RSB: stopband bandwidth/stopband center frequency
SF (Suppression Factor): Rejection Level (dB) /10
NCS: Normalized Circuit Size

TABLE III
COMPARISON BETWEEN RESULTS OF PROPOSED TUNABLE LPF AND OTHER STUDIES

Refs	f_c (GHz)	T-R %	Size (mm^2)	Tuning devices	IL (dB)
This work	0.48-1.7	71	26.8×12.8	2	0.2-1.1
[9]	1-2.2	54.5	—	4	0.6
[10]	1.5-2.5	40	15×20	2	—
[11]	1.29-2.13	39.5	—	2	0.7
[12]	1.6-2.94	46	7.7×3.5	5	0.3-0.8

frequency for the proposed LPF is 2.24 GHz. The wide stopband, ranging from 2.24 to 18 GHz, with a 22 dB rejection level gives it an edge over previous works. Furthermore, it has a far greater FOM value and the ROR parameter is equal to 308.3 dB/GHz, which is very sharp and overwhelming in comparison with previous works. Table II shows the comparison of the proposed LPF with other works.

IV. FABRICATION, RESULTS AND DISCUSSION

The proposed LPF can be made tunable by introducing varactor diodes as shown in Fig. 5. SMV-1247-079LF varactor diodes (D1, D2) with a capacitance of 0.64-8.86 pF within a range of voltage variations of 8-0 volts were used. Murata 0402-GRM 5pF has been used for the DC block (C) and the Murata GRM resistance with 100 $k\Omega$ has been used for bias resistance (R bias). The simulation and measurement results for the proposed tunable LPF for three different bias states of 1, 3 and 8 volts are shown in Fig. 6. The tuning range is defined as [12]:

$$\text{TUNING RANGE(TR)} = \frac{f_H - f_L}{f_H} \times 100\% \qquad (21)$$

In this equation, f_H is the maximum cut-off frequency among all adjustability states, and f_L is the lowest one. According to Fig. 6, it can be noticed that the tuning range

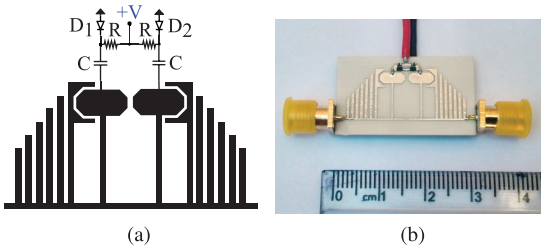

Fig. 5. Tunable LPF (a) Layout, (b) Fabricated Sample.

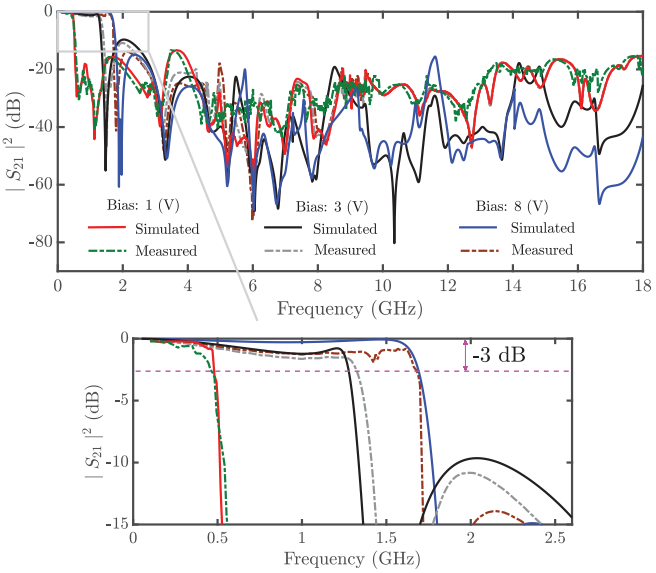

Fig. 6. Tunable LPF; simulation and measurement results.

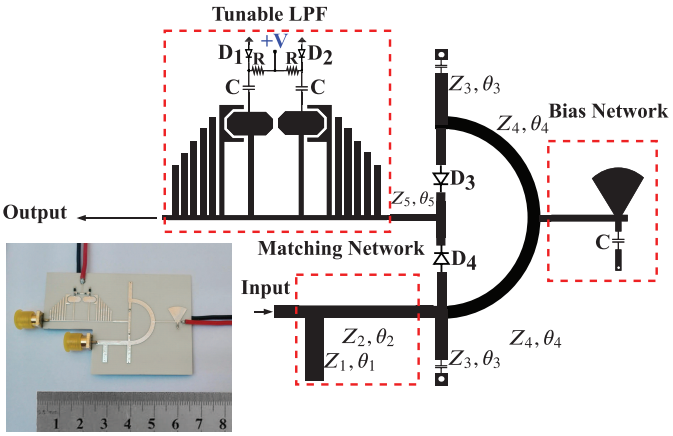

Fig. 7. Proposed detector ($Z_1 = 45\Omega, \theta_1 = 70°, Z_2 = 50\Omega, \theta_2 = 85°, Z_3 = 55\Omega, \theta_3 = 73°, Z_4 = 50\Omega, \theta_4 = 90°, Z_5 = 77\Omega, \theta_5 = 54°$); fabricated sample.

of 3 dB cut-off frequency for the proposed tunable LPF is 0.48-1.7 GHz (71%). The cut-off frequency drops as a result of introducing the tunable section. Table III shows the comparison between the proposed tunable LPF and the properties of previous works. The proposed tunable LPF has the highest percentage of the tuning range.

V. INTEGRATION WITH ENVELOPE DETECTOR

To evaluate the performance of the proposed LPF in real-time, an envelope detector shown in Fig. 7 is designed

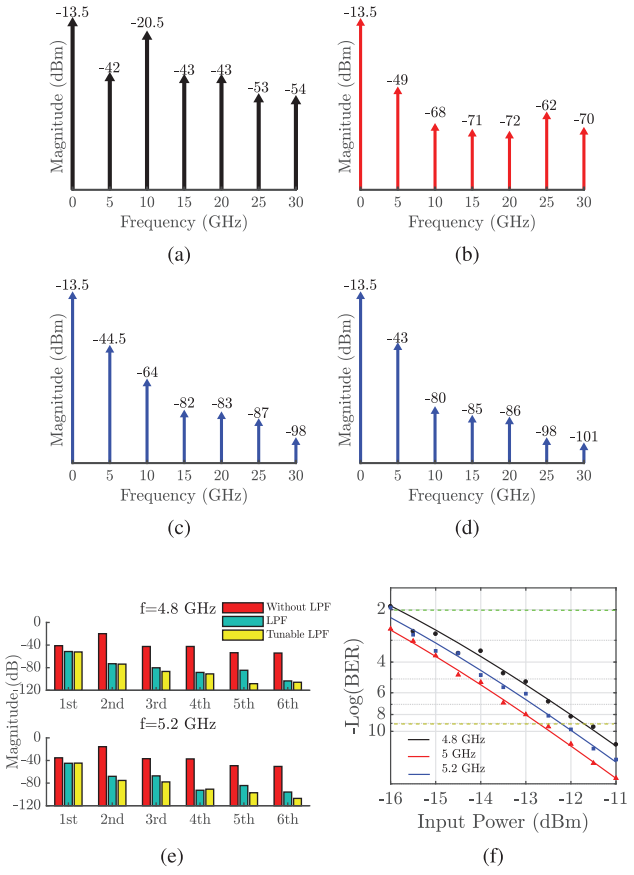

Fig. 8. Harmonic balance of the detector (a) without LPF, (b) with LPF (c) with Tunable LPF (Bias:+8v) (d) with Tunable LPF (Bias:0v) (e) harmonic suppression @ f = 4.8 and 5.2GHz. (f) BER vs input power (data markers show measurement results and the solid lines indicate corresponding interpolated values).

for the demodulation of Amplitude-shift keying (ASK) signals [16]. The detector architecture proposed is composed of two SMS7630 Schottky diodes (D3 and D4) in a balanced configuration, two shorted-stubs and a transmission line with an electrical length of 180° at $f = 5$ GHz. Furthermore, to achieve the appropriate impedance matching between RF input signal and diodes, the L-shaped matching network is used. The proposed LPF is used to obtain a flat (DC) output and also acceptable harmonics suppression. The ability of harmonic suppressing of the proposed LPF and the tunable LPF is investigated through harmonic balance analysis as shown in Fig. 8, which covers six harmonics of the fundamental frequency. Based on results in Fig. 8(a-d), one can conclude that integrating the balanced detector by the proposed LPF could suppress the harmonics considerably. The tunable LPF provides better control over higher order harmonics in comparison to the fixed LPF. This can better be understood by comparing the harmonic suppression capability of the fixed and tunable LPF in two adjacent frequency bands (4.8 GHz, 5.2 GHz) as illustrated in Fig. 8(e). Clearly, the proposed tunable LPF creates high suppressions in higher frequencies, 2nd to 6th harmonics, i.e., 5 to 30 GHz. Also, to investigate the performance of the proposed envelope detector structure from the signal integrity point of view, the bit error ratio (BER) measurement was conducted according to [16] which is shown in Fig. 8(f).

VI. Conclusion

In this brief, a novel tunable LPF with wide stopband and very sharp ROR is presented. To achieve sharp ROR and wide stopband, two hexagonal-shaped resonators and suppressing cells consisting of multi open stubs are used. The ROR parameter is very sharp and equal to 308.3 dB/GHz, which is considerably high in comparison with previous works. The proposed LPF has −3dB cutoff frequency of 2.2 GHz and the tuning range of 3 dB cut-off frequency is equal to 1.7 GHz (71%). The proposed detector architecture (with LPF) creates high harmonic suppression. Due to the aforementioned properties, the proposed LPF may find promising applications in modern communication systems.

References

[1] J. S. G. Hong and M. J. Lancaster, *Microstrip Filters for RF/Microwave Applications*, vol. 167. Hoboken, NJ, USA: Wiley, 2004.

[2] A. Sheikhi, A. Alipour, and A. Mir, "Design and fabrication of an ultra-wide stopband compact bandpass filter," *IEEE Trans. Circuits Syst. II, Exp. Briefs*, vol. 67, no. 2, pp. 265–269, Feb. 2020.

[3] C.-J. Chen, "Design of Artificial Transmission Line and Low-Pass Filter Based on Aperiodic Stubs on a Microstrip Line," *IEEE Trans. Compon. Packag. Technol.*, vol. 4, no. 5, pp. 922–928, May 2014.

[4] S. Cao, Y. Han, H. Chen, and J. Li, "An ultra-wide stop-band LPF using asymmetric Pi-shaped koch fractal DGS," *IEEE Access*, vol. 5, pp. 27126–27131, 2017.

[5] L. Kumar and M. S. Parihar, "Compact hexagonal shape elliptical low pass filter with wide stop band," *IEEE Microw. Wireless Compon. Lett.*, vol. 26, no. 12, pp. 978–980, Dec. 2016.

[6] F.-C. Chen, H.-T. Hu, J.-M. Qiu, and Q.-X. Chu, "High-selectivity low-pass filters with ultrawide stopband based on defected ground structures," *IEEE Trans. Compon. Packag. Technol.*, vol. 5, no. 9, pp. 1313–1319, Dec. 2015.

[7] A. Sheikhi, A. Alipour, and A. Abdipour, "Design of compact wide stop-band microstrip low-pass filter using T-shaped resonator," *IEEE Microw. Wireless Compon. Lett.*, vol. 27, no. 2, pp. 111–113, Feb. 2017.

[8] A. Zakharov, S. Rozenko, and M. Ilchenko, "Varactor-tuned microstrip bandpass filter with loop hairpin and combline resonators," *IEEE Trans. Circuits Syst. II, Exp. Briefs*, vol. 66, no. 6, pp. 953–957, Jun. 2019.

[9] L. Kumar and M. S. Parihar, "A compact reconfigurable low-pass filter with wide-stopband rejection bandwidth," *IEEE Microw. Wireless Compon. Lett.*, vol. 28, no. 5, pp. 401–403, May 2018.

[10] A. Abbosh, "Compact tunable low-pass filter using variable mode impedance of coupled structure," *IET Microw. Antennas Propag.*, vol. 6, no. 12, pp. 1306–1310, Sep. 2012.

[11] C.-C. Huang, N.-W. Chen, H.-J. Tsai, and J.-Y. Chen, "A coplanar waveguide bandwidth-tunable lowpass filter with broadband rejection," *IEEE Microw. Wireless Compon. Lett.*, vol. 23, no. 3, pp. 134–136, Mar. 2013.

[12] J. Ni and J. Hong, "Compact continuously tunable microstrip low-pass filter," *IEEE Trans. Microw. Theory Techn.*, vol. 61, no. 5, pp. 1793–1800, May 2013.

[13] M. Hayati, S. Zarghami, and A. H. Kazemi, "Very sharp roll-off ultra-wide stopband low-pass filter using modified flag resonator," *IEEE Trans. Compon. Packag. Technol.*, vol. 8, no. 12, pp. 2163–2170, Dec. 2018.

[14] G. Moloudian and M. Dousti, "Design and fabrication of a compact microstrip lowpass-bandpass diplexer with high isolation for telecommunication applications," *Int. J. RF Microw. Comput.-Aided Eng.*, vol. 28, no. 5, pp. 21248–21258, 2018.

[15] M. Kirschning, R. H. Jansen, and N. H. L. Koster, "Measurement and computer-aided modeling of microstrip discontinuities by an improved resonator method," in *IEEE MTT-S Int. Microw. Symp. Dig.*, Boston, MA, USA, Jun. 1983, pp. 495–497.

[16] A. B. Granja *et al.*, "Compact high-speed envelope detector architecture for ultra-wideband communications," *Microw. Opt. Technol. Lett.*, vol. 60, no. 4, pp. 936–941, Apr. 2018.